LETTERS

Hydrous silicate melt at high pressure

Mainak Mookherjee[1], Lars Stixrude[2] & Bijaya Karki[3]

The structure and physical properties of hydrous silicate melts and the solubility of water in melts over most of the pressure regime of Earth's mantle (up to 136 GPa) remain unknown. At low pressure (up to a few gigapascals) the solubility of water increases rapidly with increasing pressure[1], and water has a large influence on the solidus temperature, density[2], viscosity[3] and electrical conductivity. Here we report the results of first-principles molecular dynamics simulations of hydrous $MgSiO_3$ melt. These show that pressure has a profound influence on speciation of the water component, which changes from being dominated by hydroxyls and water molecules at low pressure[4] to extended structures at high pressure. We link this change in structure to our finding that the water–silicate system becomes increasingly ideal at high pressure: we find complete miscibility of water and silicate melt throughout almost the entire mantle pressure regime. On the basis of our results, we argue that a buoyantly stable melt at the base of the upper mantle would contain approximately 3 wt% water and have an electrical conductivity of 18 S m^{-1}, and should therefore be detectable by means of electromagnetic sounding.

The hydrogen bond is not well described by the dominantly ionic, atomistic models that have most often been applied to the study of silicate melts. First-principles molecular dynamics simulations are more costly in terms of computer time but have the important advantage of making no a priori assumptions regarding the nature of the bonding or the shape of the charge density. Density functional theory, on which our simulations are based, has been successfully applied to the study of a number of hydrous crystalline silicates and oxides[5] and to the liquid SiO_2-H_2O system at ambient pressure[6].

In our first-principles molecular dynamics simulations of a hydrous $MgSiO_3$-H_2O liquid with 10 wt% water, the electronic structure, the Hellman–Feynman forces acting on the nuclei, and thermodynamic properties are computed at each time step in the local density and pseudopotential approximations. Atomic trajectories extracted from the simulations reveal the structure, speciation and dynamics of the melt. To quantify the influence of the water component on physical properties, we compare our results with a previous first-principles molecular dynamics study of anhydrous $MgSiO_3$ liquid[7].

Inspection of the equilibrated liquid structure shows that pressure has a large influence on the speciation of the water component (Fig. 1). Whereas at low pressure we find mostly hydroxyls and water molecules, at high pressure we see a much greater variety of species. These include Si–O–H–O–Si polyhedral linkages, –O–H–O–H– chains and O–H–O edge decoration of SiO_6 octahedra, the last of which was suggested in a previous experimental study of glasses[8]. We note another feature at low pressure that had not been anticipated experimentally: a strong preference for water molecules to bond to Mg^{2+} cations. This chemical association, together with the decrease in the proportion of hydroxyls with increasing pressure, may explain the increase in the MgO/SiO_2 ratio of eutectic melts in the MgO-SiO_2-H_2O system with increasing pressure up to 15 GPa (ref. 9).

The water component becomes more interconnected with increasing pressure, transforming from isolated molecular species at low pressure to a structure more reminiscent of bulk phases of water at higher pressure (Fig. 2a). The H–O coordination number varies in value from almost one at low pressure to two at the highest pressures investigated. This coordination number is similar to that in the high-pressure form of water[10] and in ice in which the structure is a complete three-dimensional network of nearly symmetric hydrogen bonds (ice X). Simultaneously, as compression increases, the very open silica framework gives way to a much more densely packed structure in which little free volume remains to accommodate highly polar molecular species: molecules are squeezed out as pressure increases, and are replaced by extended structures.

The addition of water disrupts the intermediate-range silicate structure: the O–Si coordination number of the hydrous melt is substantially less than that of the anhydrous melt, demonstrating that added water disrupts interpolyhedral linkages (Fig. 2b). Such disruption is consistent with experimental evidence at low pressure for the decrease in viscosity with increasing water content in silicate melts. Because we find water-induced disruption of the silicate network at all pressures, we anticipate that addition of water will decrease the viscosity of silicate melts at high pressure as well. In contrast, the Si–O coordination number in hydrous and anhydrous melts is identical at all pressures. Mg–O coordination numbers are similarly unaffected by the addition of water at pressures greater than 20 GPa; at lower pressures the addition of water decreases the Mg–O coordination number through the interaction of water molecules with Mg cations.

We find that protons are highly mobile, presenting a possible means of geophysical detection of deep melt. The diffusivity of hydrogen is an order of magnitude greater than that of the other ions. From our simulations, D, the self-diffusion coefficient of hydrogen, is adequately described by the Arrhenius relation (Fig. 3)

$$D = D_0 \exp\left(-\frac{E^* + PV^*}{kT}\right) \quad (1)$$

where E^* denotes the activation energy, V^* denotes the activation volume, T denotes the temperature, P denotes the pressure, D_0 denotes the value of D in the limit of infinite temperature and k denotes the Boltzmann constant. The electrical conductivity σ due to charged mobile species is given by the Nernst–Einstein relation

$$\sigma = \frac{Dxq^2}{kTH_R} \quad (2)$$

where x is the number of carriers per unit volume, the Haven ratio H_R approaches a value of one for small values of x (ref. 11) and q is the electrical charge of the carrier.

Assuming that protons are the primary charge carriers and that $H_R = 1$, from equations (1) and (2) we estimate a conductivity of $59c/10$ S m^{-1} under conditions thought to represent the mantle at a depth of 410 km (that is, a pressure of 14 GPa and a temperature of

[1]Department of Geology and Geophysics, Yale University, New Haven, Connecticut 06511, USA. [2]Department of Earth Sciences, University College London, Gower Street, London WC1E 6BT, UK. [3]Department of Computer Science and Department of Geology and Geophysics, Louisiana State University, Baton Rouge, Louisiana 70803, USA.

1,800 K), where c is the percentage mass fraction of water in the melt. This corresponds to approximately 18 S m^{-1} for a neutrally buoyant melt, which at this depth has $c = 3$ wt% (see below). The electrical conductivity of hydrous silicate melt has not been measured at pressures greater than 1 GPa. Because the expected water concentration in the solid mantle on either side of a hydrous melt layer is much less than 1%, the melt layer would represent a large conductance anomaly (of 18,000 S, assuming that $\sigma = 18$ S m^{-1} and there is a 20-km-thick partial melt layer with 5% neutrally buoyant hydrous melt[12]) that should be detectable by means of electromagnetic sounding. Indeed, recent inversions of electromagnetic data, although non-unique, fit a value of total conductance similar to the values we find[13].

The equation of state of the hydrous liquid, like that of the anhydrous liquid, differs from that of most crystalline mantle phases in an important way: the thermal pressure increases markedly on compression (Fig. 4). The hydrous liquid equation of state can be described by the Mie–Grüneisen form

$$P(V,T) = P_c(V,T) + \frac{\gamma}{V} C_v(T - T_o)$$

where P_c denotes the reference isotherm, taken to lie at $T_o = 3{,}000$ K, γ denotes the Grüneisen parameter and C_v denotes the isochoric heat capacity. These quantities are obtained from the simulation: as the internal energy E and pressure P vary linearly with temperature along isochores (to within our uncertainty), the values are calculated at each volume from $\gamma = V(\partial P/\partial E)_V$ and $C_v = (\partial E/\partial T)_V$. The isochoric heat capacity decreases by about 8% upon twofold compression, from $3.63 \pm 0.21\,Nk$ to $3.34 \pm 0.11\,Nk$, where N is the number of atoms. The value of γ increases by a factor of three over the same compression range. This behaviour is opposite to that of mantle

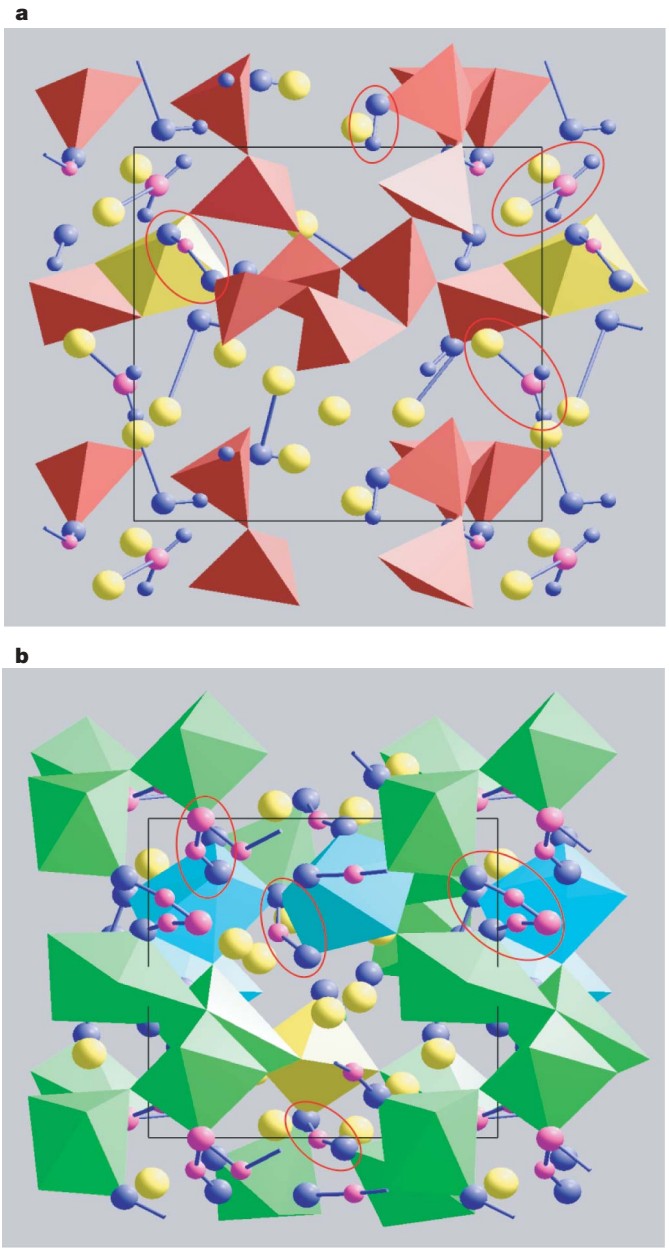

Figure 1 | Structure and speciation of hydrous silicate melt. **a**, 3,000 K, $V/V_x = 1$; **b**, 3,000 K, $V/V_x = 0.5$. Red, yellow, green and cyan polyhedra represent four-, five-, six- and sevenfold Si–O coordination environments, respectively. Yellow spheres represent Mg atoms. Other spheres represent H atoms (small spheres) and those O atoms (large spheres) not solely bonded to Si; they are coloured pink if they are bonded to at least two other H atoms or O atoms, and are coloured blue if they are bonded to only one other H or O atom. Red ellipses highlight species discussed in the text, including hydroxyls (O–H in **a**), water molecules bound to Mg ions (Mg–O–H_2 in **a**), interpolyhedral bridges (Si–O–H–O–Si in **b**), polyhedral edge decoration (O–H–O in **b**) and a Si–O–H–O–H–O–Si interpolyhedral bridge (in **b**). The apparent equilibrium constant of the reaction[4] $H_2O + O = 2OH^-$ at 3,000 K and near-ambient pressure computed from our simulations is 3.1, which is in close agreement with the value (2.3) extrapolated from experimental measurements on rhyolite compositions[27] at much lower temperatures and water contents, and is consistent with the experimentally observed tendency of water molecules increasingly to dissociate in the melt as temperature increases. The molecular dynamics snapshots were rendered using the visualization system of Bhattarai *et al.*[28]. In each panel, the black outline represents the primary simulation cell.

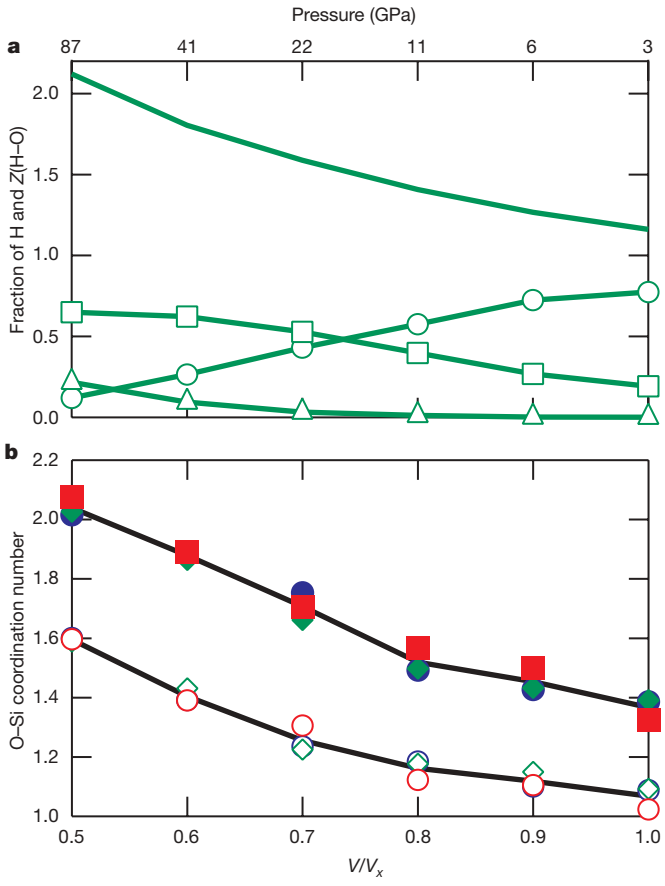

Figure 2 | H–O and O–Si coordination numbers. **a**, Fraction of protons bonded to one (open circles), two (squares) and three (triangles) O atoms, and the mean H–O coordination number Z(H–O) (solid line without symbols) at 4,000 K. The simulated pressure at 4,000 K is indicated along the top axis. **b**, Evolution of O–Si coordination number upon compression, for anhydrous[7] (filled symbols) and hydrous (open symbols) melts at 3,000 K (blue), 4,000 K (green) and 6,000 K (red). Black lines represent temperature-averaged values.

crystalline phases and similar to that of anhydrous $MgSiO_3$ liquid[7]: within our uncertainty, the values of γ for hydrous and anhydrous melts are identical over the entire volume range explored.

The density of the hydrous melt is less than that of the anhydrous melt under all conditions explored here (Fig. 4a), but the density contrast is small enough that hydrous melts may be neutrally buoyant in the mantle, providing a possible explanation of a low-velocity layer found on top of the 410-km discontinuity[12]. The density contrast is remarkably constant across the pressure–temperature range of the mantle, varying from 0.3 to 0.4 g cm^{-3} between 1 and 100 GPa and 3,000 and 6,000 K. We estimate the amount of water that would produce a neutrally buoyant melt at a depth of 410 km as $c/10 = (\rho_{410} - \rho_{\mathrm{anhydrous}})/\Delta\rho_{H_2O}$, where $\rho_{410} = 3.54$ g cm^{-3} is the density at the base of Earth's upper mantle[14], $\rho_{\mathrm{anhydrous}} = 3.66$ g cm^{-3} is the density of a partial melt of anhydrous peridotite[15] at 13.4 GPa and 1,873 K, and $\Delta\rho_{H_2O} = -0.35$ g cm^{-3} is the density contrast that we find for 10 wt% water. We find from this analysis that $c = 3$ wt%, consistent with recent estimates[16,17].

The partial molar volume of water in the silicate melt, $\bar{V}_{H_2O}$, asymptotically approaches that of pure water, V_{H_2O}, as pressure increases (Fig. 4b). At the highest pressure that we studied, $\bar{V}_{H_2O}$ and V_{H_2O} are identical to within our uncertainty. This means that the volume of solution ΔV, which is large and negative at low pressure, approaches the ideal limit ($\Delta V \rightarrow 0$) as pressure increases. The increasing similarity of the volumes of water in the melt and in pure form is consistent with our finding that the water component becomes more structurally interconnected and more like bulk water with increasing pressure. An important consequence of the increasing ideality of the water–silicate solution with increasing pressure is the almost constant density of hydration that we find (Fig. 4a): if $\Delta V = 0$ at all pressures, the density contrast between hydrous and anhydrous melts varies rapidly with pressure at low pressure.

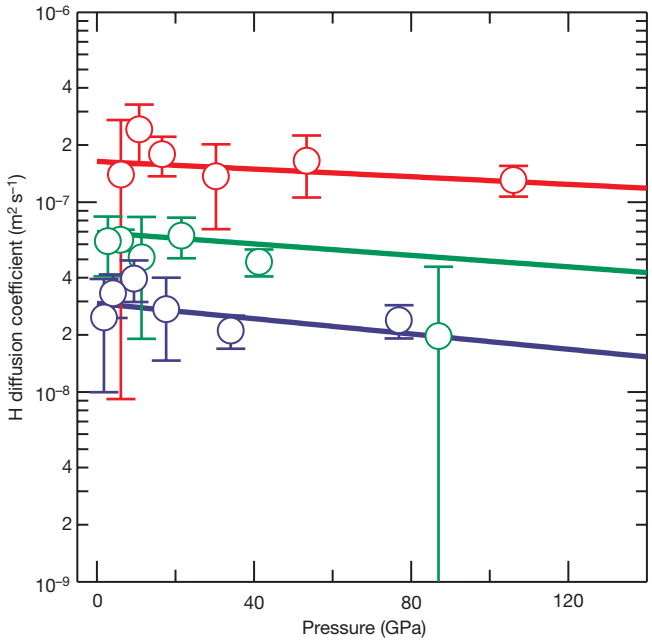

Figure 3 | Self-diffusion coefficient of hydrogen. Results at 3,000 K (blue), 4,000 K (green) and 6,000 K (red) from our simulations (symbols) and an Arrhenius fit to the simulation results (lines) (equation (1) with $D_0 = 9.2 \times 10^{-7}$ m^2 s^{-1}, $E^* = 86$ kJ mol^{-1} and $V^* = 0.11$ cm^3 mol^{-1}). The value of the activation energy is similar to that found in hydrous basaltic melts at low pressure[29] (126 ± 32 kJ mol^{-1}), and the value of the diffusivity agrees well with that extrapolated to 3,000 K from lower temperature, low-pressure experiments[29] (2.4×10^{-8} m^2 s^{-1}), indicating that proton diffusion does not depend strongly on melt composition. Error bars represent one-s.d. uncertainties.

We predict that the solubility of water in silicate melt will increase as pressure increases and will be essentially unlimited at all mantle pressure–temperature conditions beyond a few gigapascals. This prediction is based on our finding that the water component behaves increasingly ideally as pressure increases. The volume of solution $\Delta V = \mathrm{d}(\Delta G)/\mathrm{d}P$ is ≤ 0 at all pressures investigated, so the Gibbs free energy of solution ΔG, which limits solubility, must decrease to a small, pressure-independent value as pressure increases to around 100 GPa, where ΔV vanishes. As ΔG is sufficiently small to permit complete solubility at 12 GPa (ref. 18), solubility must remain undiminished as pressure increases to at least the highest pressure we study here (100 GPa). The dependence of $\bar{V}_{H_2O}$ on silicate composition remains to be investigated at high pressure. However, we note that $\bar{V}_{H_2O}$ is apparently very insensitive to silicate composition at low pressure[2], indicating that our arguments regarding solubility may be applicable to natural melt compositions as well.

Essentially unlimited solubility of water in silicate melt over most of the mantle regime would have potentially important implications for our understanding of Earth's origins. In most models of the accreting Earth, a deep magma ocean, possibly encompassing the entire mantle, is an important reservoir of water. Our results show

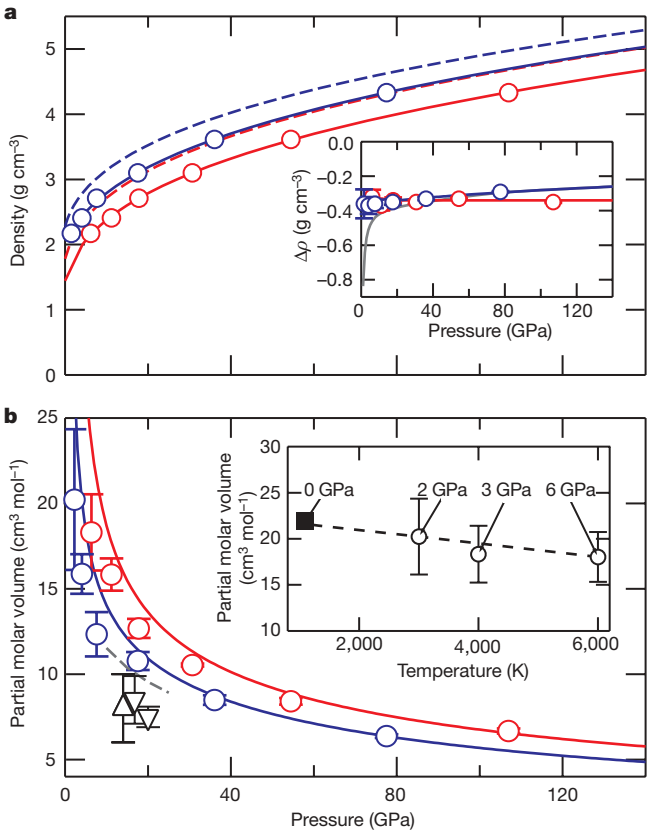

Figure 4 | Density and partial molar volume of water. a, Comparison of the density of hydrous (solid lines with symbols) and anhydrous[7] (dashed lines) melts along 3,000 K (blue) and 6,000 K (red) isotherms. The inset shows the density contrast between hydrous and anhydrous melt along 3,000 K (blue) and 6,000 K (red) isotherms. For comparison, the grey line shows the density contrast between an anhydrous melt and an ideal hydrous melt ($\Delta V = 0$) at 3,000 K. **b**, Partial molar volume of water from our simulations at 6,000 K (red circles) and 3,000 K (blue circles), compared with that of pure water[30] (solid lines). The partial molar volumes of water derived from high-pressure experiments (upward triangle[16] and downward triangles[17]) are shown for comparison. The dashed line represents the partial molar volume from this study extrapolated to 2,200 K, the experimental temperature in refs 16 and 17. The inset shows the partial molar volume of water (open circles) that we calculate extrapolated along the isochore $V/V_x = 1$ to zero pressure (dashed line), in excellent agreement with experiment (solid square[2]). Error bars represent one-s.d. uncertainties.

that this reservoir could easily store all the water delivered to Earth (probably bounded by the 5–7% by mass present in CI carbonaceous chondrites[19]), which probably exceeds the amount of water in the present Earth (0.005–0.02% by mass in the source of mid-ocean-ridge basalts[20]) by a large factor. Moreover, water stored in the magma ocean may have fundamentally altered its thickness, thermal state and dynamics, by means of water-induced lowering of the solidus and the viscosity. Extensive solubility of water in the early magma ocean may have had important implications for the origin of the hydrosphere[21].

METHODS SUMMARY

The simulations were performed in the canonical ensemble with periodic boundary conditions and a Nosé thermostat[22]. The primary cell contained 84 atoms (12 $MgSiO_3$ molecules and eight water molecules: 10 wt% water). As our initial condition, a pyroxene structure with water molecules placed in the vacant space between tetrahedral chains and in the *b*–*c* plane was homogeneously strained to a cubic shape and the desired volume. The system was melted at 6,000 K and then cooled isochorically to first 4,000 K and then 3,000 K. We used a time step of 0.5 fs. Total run durations were 3 ps at 6,000 K, 4.5 ps at 4,000 K (except for V/V_x values of 0.5 and 0.6, for which the duration was 6 ps) and 6 ps at 3,000 K (except for a V/V_x value of 0.6, for which the duration was 12.5 ps, and a V/V_x value of 0.5, for which the duration was 15 ps). In all cases the final 80% of the trajectories were used to compute averages.

Self-diffusion coefficients were determined from the slope of the linear portion of the plot of mean squared displacement versus time (see the Supplementary Information). We confirmed that the simulated properties were not significantly affected if we doubled the cell size or used a different initial condition. We used ultrasoft pseudopotentials[23] and VASP[24], computing the electronic structure at the Brillouin zone centre with an energy cutoff of 400 eV. Pulay corrections to the pressure were estimated to be the same as in the anhydrous case[7], varying linearly from 2 GPa at $V = V_x$ to 5 GPa at $V = V_x/2$, where $V_x = 1{,}033.54$ Å^3 per simulation cell (84 atoms), identical to the reference volume of our anhydrous simulations. To account for the error inherent in the approximation to the exchange correlation functional, we added a uniform correction of 2 GPa to the pressure[7]. The simulations were confined to the Born–Oppenheimer surface and include the influence of the finite temperature through the Mermin functional[25,26].

Received 12 October 2007; accepted 17 March 2008.

1. Shen, A. H. & Keppler, H. Direct observation of complete miscibility in the albite-H_2O system. *Nature* **385,** 710–712 (1997).
2. Ochs, F. A. & Lange, R. A. The density of hydrous magmatic liquids. *Science* **283,** 1314–1317 (1999).
3. Lange, R. A. The effect of H_2O, CO_2 and F on the density and viscosity of silicate melts. *Rev. Mineral.* **30,** 331–369 (1994).
4. Stolper, E. The speciation of water in silicate melts. *Geochim. Cosmochim. Acta* **46,** 2609–2620 (1982).
5. Panero, W. R. & Stixrude, L. P. Hydrogen incorporation in stishovite at high pressure and symmetric hydrogen bonding in delta-AlOOH. *Earth Planet. Sci. Lett.* **221,** 421–431 (2004).
6. Pohlmann, M., Benoit, M. & Kob, W. First-principles molecular-dynamics simulations of a hydrous silica melt: Structural properties and hydrogen diffusion mechanism. *Phys. Rev. B* **70,** 184209 (2004).
7. Stixrude, L. & Karki, B. Structure and freezing of $MgSiO_3$ liquid in Earth's lower mantle. *Science* **310,** 297–299 (2005).
8. Closmann, C. & Williams, Q. In-situ spectroscopic investigation of high-pressure hydrated (Mg,Fe)SiO_3 glasses - OH vibrations as a probe of glass structure. *Am. Mineral.* **80,** 201–212 (1995).
9. Inoue, T. Effect of water on melting phase relations and melt composition in the system Mg_2SiO_4-$MgSiO_3$-H_2O up to 15 GPa. *Phys. Earth Planet. Inter.* **85,** 237–263 (1994).
10. Goldman, N., Fried, L. E., Kuo, I. F. W. & Mundy, C. J. Bonding in the superionic phase of water. *Phys. Rev. Lett.* **94,** 217801 (2005).
11. Greaves, G. N. & Ngai, K. L. Reconciling ionic-transport properties with atomic-structure in oxide glasses. *Phys. Rev. B* **52,** 6358–6380 (1995).
12. Song, T. R. A., Helmberger, D. V. & Grand, S. P. Low-velocity zone atop the 410-km seismic discontinuity in the northwestern United States. *Nature* **427,** 530–533 (2004).
13. Toffelmier, D. A. & Tyburczy, J. A. Electromagnetic detection of a 410-km-deep melt layer in the southwestern United States. *Nature* **447,** 991–994 (2007).
14. Dziewonski, A. M. & Anderson, D. L. Preliminary reference earth model. *Phys. Earth Planet. Inter.* **25,** 297–356 (1981).
15. Ito, E. & Takahashi, E. Melting of peridotite at uppermost lower-mantle conditions. *Nature* **328,** 514–517 (1987).
16. Matsukage, K. N., Jing, Z. C. & Karato, S. Density of hydrous silicate melt at the conditions of Earth's deep upper mantle. *Nature* **438,** 488–491 (2005).
17. Sakamaki, T., Suzuki, A. & Ohtani, E. Stability of hydrous melt at the base of the Earth's upper mantle. *Nature* **439,** 192–194 (2006).
18. Stalder, R., Ulmer, P., Thompson, A. B. & Gunther, D. High pressure fluids in the system MgO-SiO_2-H_2O under upper mantle conditions. *Contrib. Mineral. Petrol.* **140,** 607–618 (2001).
19. Kerridge, J. F. Carbon, hydrogen and nitrogen in carbonaceous chondrites - abundances and isotopic compositions in bulk samples. *Geochim. Cosmochim. Acta* **49,** 1707–1714 (1985).
20. Hirschmann, M. M. Water, melting, and the deep Earth H_2O cycle. *Annu. Rev. Earth Planet. Sci.* **34,** 629–653 (2006).
21. Matsui, T. & Abe, Y. Evolution of an impact-induced atmosphere and magma ocean on the accreting Earth. *Nature* **319,** 303–305 (1986).
22. Nosé, S. A unified formulation of the constant temperature molecular-dynamics methods. *J. Chem. Phys.* **81,** 511–519 (1984).
23. Kresse, G. & Hafner, J. Norm-conserving and ultrasoft pseudopotentials for first-row and transition-elements. *J. Phys. Condens. Matter* **6,** 8245–8257 (1994).
24. Kresse, G. & Furthmüller, J. Efficient iterative schemes for ab initio total-energy calculations using a plane-wave basis set. *Phys. Rev. B* **54,** 11169–11186 (1996).
25. Mermin, N. D. Thermal properties of inhomogeneous electron gas. *Phys. Rev.* **137,** A1441–A1443 (1965).
26. Wentzcovitch, R. M., Martins, J. L. & Allen, P. B. Energy versus free-energy conservation in 1st-principles molecular-dynamics. *Phys. Rev. B* **45,** 11372–11374 (1992).
27. Zhang, Y. X. H_2O in rhyolitic glasses and melts: Measurement, speciation, solubility, and diffusion. *Rev. Geophys.* **37,** 493–516 (1999).
28. Bhattarai, D., Karki, B. B. & Stixrude, L. Space-time multiresolution atomistic visualization of MgO and $MgSiO_3$ liquid data. *Vis. Geosci.* **11,** 1–11 (2006).
29. Zhang, Y. X. & Stolper, E. M. Water diffusion in a basaltic melt. *Nature* **351,** 306–309 (1991).
30. Pitzer, K. S. & Sterner, S. M. Equations of state valid continuously from zero to extreme pressures for H_2O and CO_2. *J. Chem. Phys.* **101,** 3111–3116 (1994).

Supplementary Information is linked to the online version of the paper at www.nature.com/nature.

Acknowledgements Authors thank the Center for Computation & Technology at Louisiana State University for computing resources. This work was supported by the US National Science Foundation.

Author Information Reprints and permissions information is available at www.nature.com/reprints. Correspondence and requests for materials should be addressed to L.S. (stixrude@umich.edu).